Hot Carrier Extraction with Plasmonic Broadband Absorbers

Charlene Ng,[*,†,‡] Jasper J. Cadusch,[¶] Svetlana Dligatch,[§] Ann Roberts,[¶] Timothy J. Davis,[¶] Paul Mulvaney,[‖] and Daniel E. Gómez[*,†,‡]

†*CSIRO, Manufacturing, Private Bag 33, Clayton, VIC, 3168, Australia*

‡*Melbourne Centre for Nanofabrication, Australian National Fabrication Facility, Clayton VIC 3168, Australia*

¶*School of Physics, The University of Melbourne, Parkville, VIC, 3010, Australia* §*CSIRO, Manufacturing, PO Box 218, Lindfield NSW 2070, Australia*

‖*Bio21 Institute & School of Chemistry, The University of Melbourne, Parkville VIC 3010, Australia*

E-mail: charlene.ng@csiro.au; daniel.gomez@csiro.au

S1 Additional supporting figures

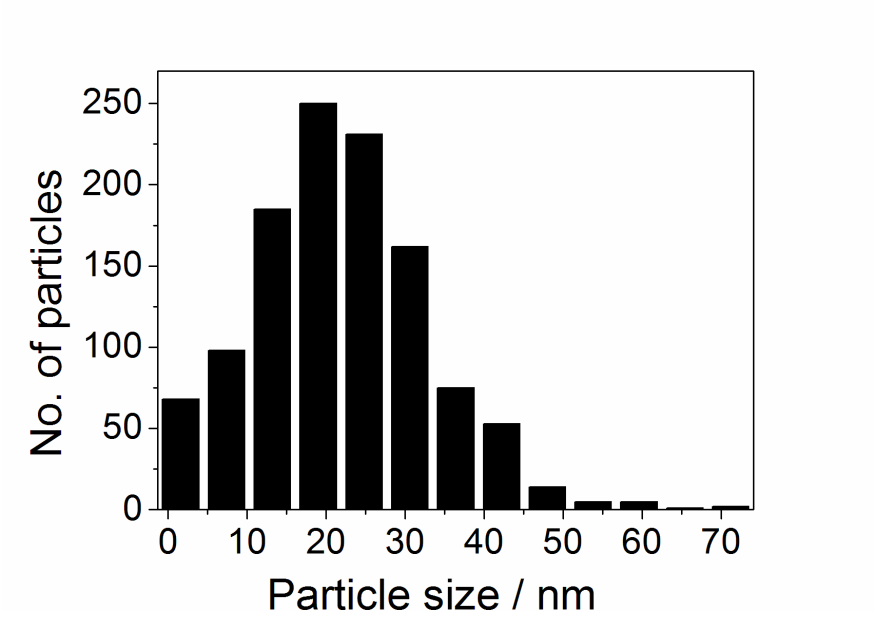

Figure S1: Measured size distribution of the Au nanoparticles.

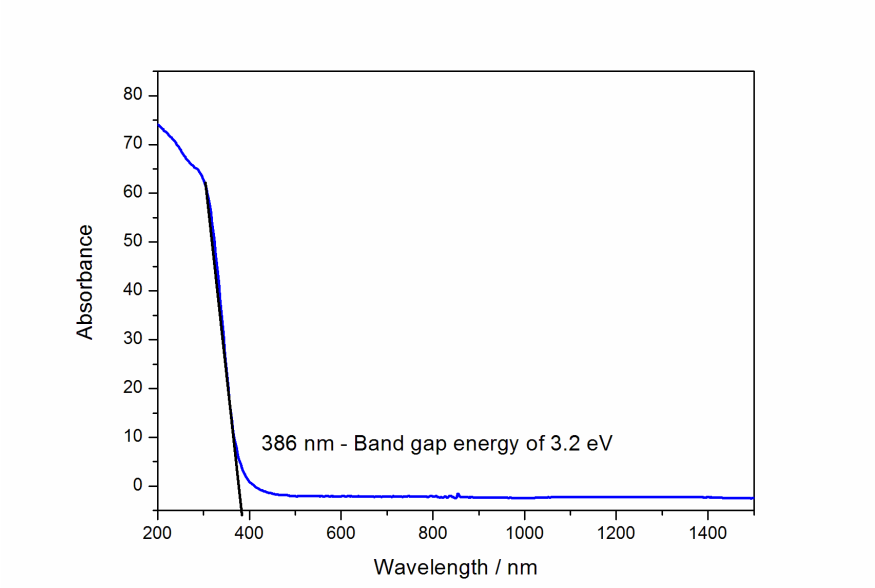

Figure S2: Absorption spectrum of the bare TiO_2 film. Analysis of these data yields a bandgap of 3.2 eV for the material as indicated.

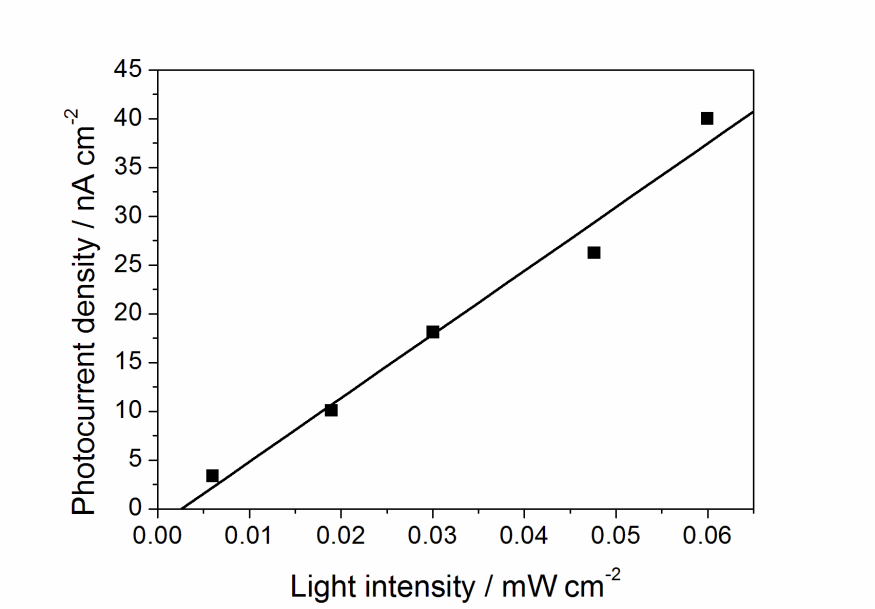

Figure S3: IPCE vs light intensity. Sample: Al/50nmTiO2/AuNP Electrolyte: 0.5M Na_2SO_4 with 20v/v% methanol Wavelength: 600 nm. Bias Voltage: 0.5 V

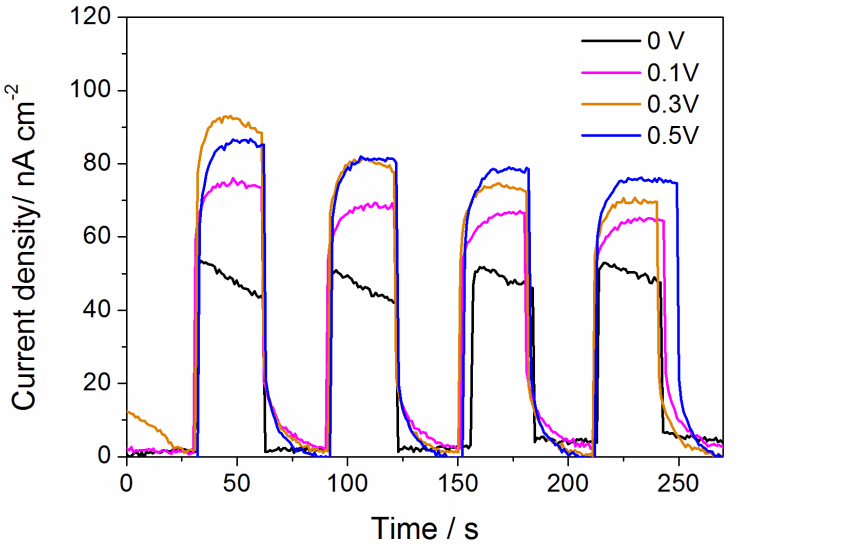

Figure S4: IPCE vs light intensity. Sample: Al/50nmTiO2/AuNP Electrolyte: 0.5M Na_2SO_4 with 20v/v% methanol Wavelength: 600 nm. Bias Voltage: 0.5 V

S2 Finite element method (FEM) calculations

The FEM calculations were carried out using COMSOL Multiphysics 5.0, using the model geometry shown in figure S5 (which also shows the the electric field). The model consists of a 500 nm x 500 nm x 2000 nm unit cell, with periodic boundary conditions on the sides and scattering boundary conditions for the top and bottom boundaries. The nanoparticle (AuNP) layer was 14 nm thick, the TiO_2 layer was allowed to have variable thickness and the reflecting mirror had a fixed thickness of 150 nm. The refractive index of Au taken from literature.[1] The AuNP layer thickness was determined by calculating the surface coverage of nanoparticles (47%) from the SEM image shown in the main text and applying volume conservation. A 7 nm solid gold film has the same volume as a 14 nm film with 47% surface coverage, so we take 14 nm as the average height of the nanoparticles. The optical constants of the TiO_2 film were taken from ellipsometry data. Illumination was modelled with a plane wave launched from the top boundary of the simulation geometry.

Figure S6 shows the scheme used to calculate the total absorption in the metal/semiconductor/metal structures and the absorption of light by the AuNP film and the reflecting layer. The first step is to convert the measured SEM image to a monochrome bitmap. A function f is then created whose value at a particular coordinate (x, y) in the image is 1 if there is gold at that location and 0 otherwise:

$$f(x,y) = \begin{cases} 0 & \text{pixel(x,y) = black,} \\ 1 & \text{pixel(x,y) = white.} \end{cases} \tag{S1}$$

With f, it is possible to define a spatially–dependent relative permittivity:

$$\epsilon(x,y,\lambda) = \epsilon_0 + f(x,y)(\epsilon_{Au}(\lambda) - \epsilon_0). \tag{S2}$$

Figure S7 shows the calculated spatial distribution of electromagnetic fields in samples

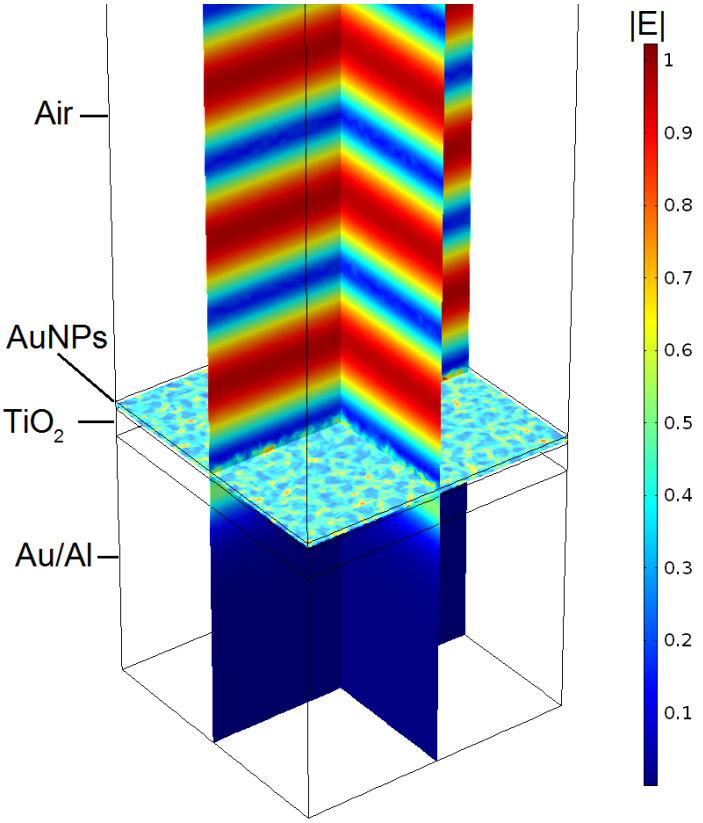

Figure S5: The FEM model geometry used to calculate the total absorption of the device and the location of the absorption. Here the normalized magnitude of the electric field is shown.

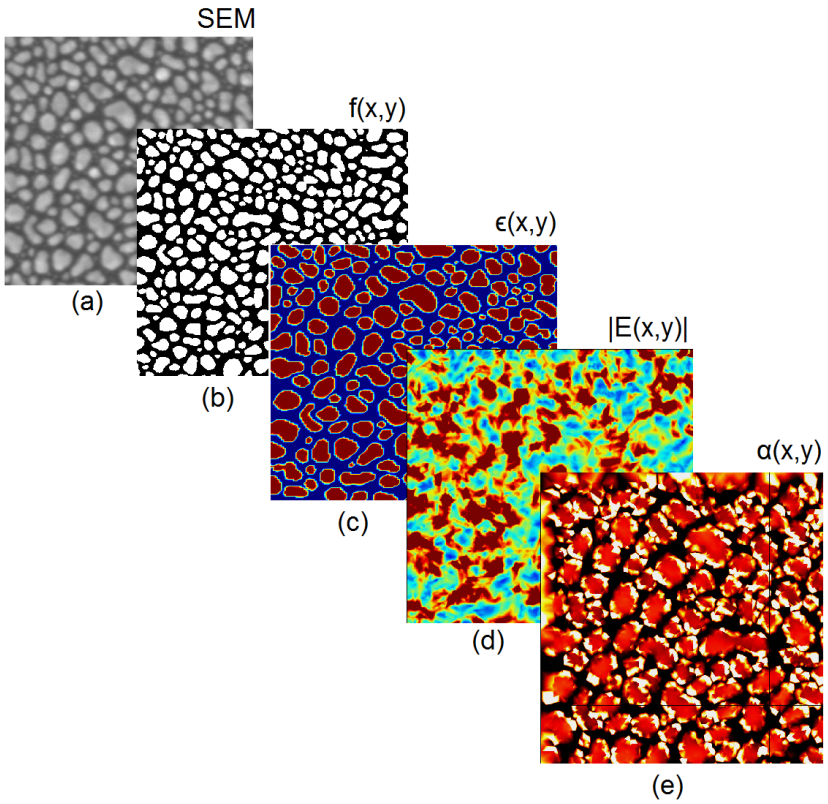

Figure S6: A scheme for calculating absorption from SEM image. Convert the SEM (a) into a monochrome bitmap (b), then use this to define a material with (x,y), a spatially dependant relative permittivity, (c). This material can then be used in FEM calculations to determine the electric field (d) and thus the electromagnetic absorption, α, in the layer (e).

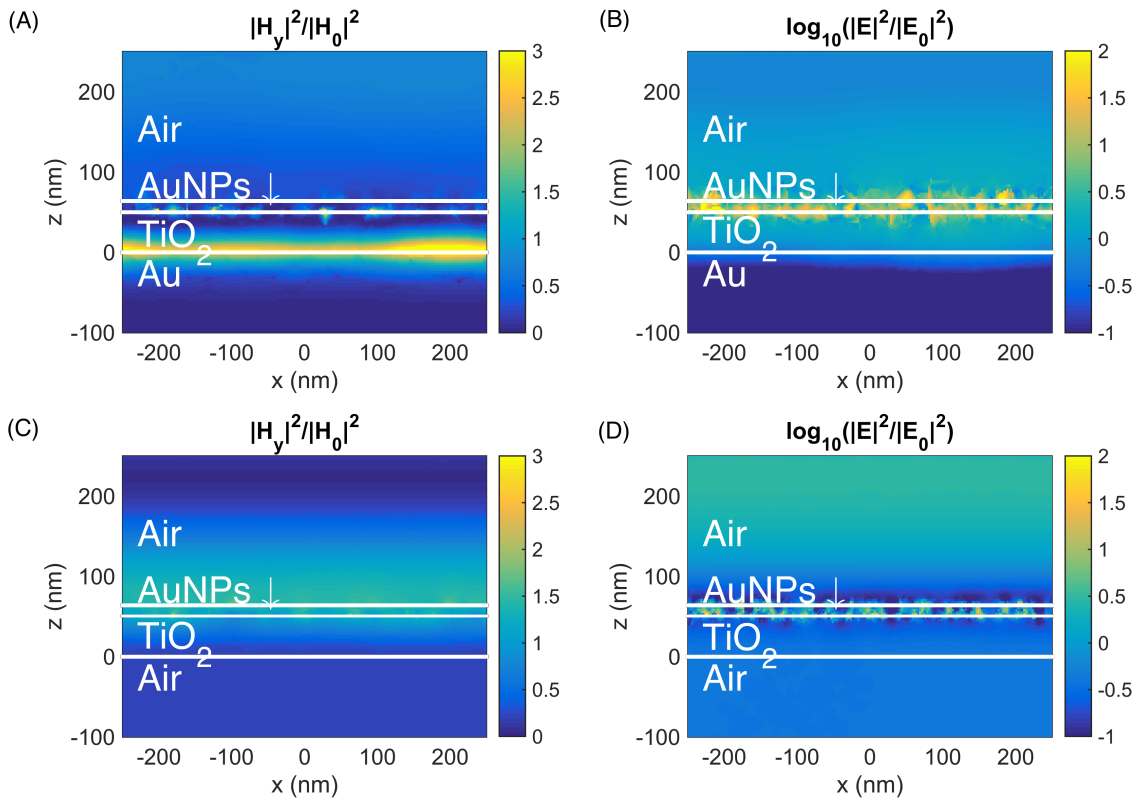

Figure S7: spatial distribution of electromagnetic fields in samples with (A,B) and without (C,D) a metal reflecting layer for a wavelength of 600 nm.

with and without a metal reflecting layer.

S3 Model of the internal quantum efficiency η

We consider a top illuminated metal/semiconductor/metal–nanoparticle structure, where the top metal layer consists of metal nanoparticles. This top layer forms a Schottky contact with the semiconductor with a barrier height Φ_{SB} (we ignore Fermi pinning effects or any other effects due to surface imperfections), and we describe in this section the electron flow that originates from the nanoparticles (possible thermally activated charge flow on the opposite direction is not considered).

The incident photon–to–electron conversion efficiency is described, to a good level of accuracy, by the product of the absorption efficiency $A(\lambda)$ of the top layer and the internal quantum efficiency $\eta(\lambda)$ for detecting a hot charge carrier per each absorbed photon:

$$\mathrm{IPCE}(\lambda) = A(\lambda)\eta(\lambda). \tag{S3}$$

η is approximated as the following product:

$$\eta = \eta_{\mathrm{inj}} \times \eta_{\mathrm{trpt}} \times \eta_{\mathrm{injm}} \times \eta_{ed}, \tag{S4}$$

where:

- η_{inj}: the injection efficiency of hot electrons into the semiconductor material,
- η_{trpt} the probability that the electron travels through the semiconductor into the second interface,
- η_{injm} the transmission coefficient for electrons travelling from the semiconductor into the metal electrode/reflector and,
- η_{ed} the efficiency of the redox processes that lead to charge injection from species in solution to positively charged Au nanoparticles.

We now consider each of these processes in detail.

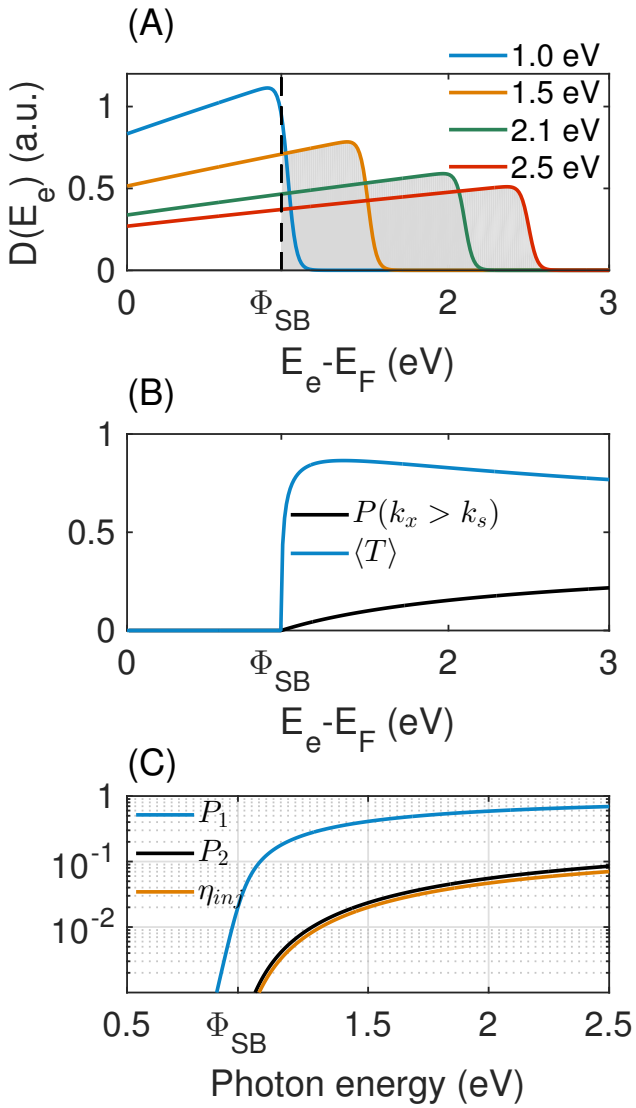

Figure S8: Injection efficiency. (A) Energy distribution of photo–excited electrons. The horizontal scale represents the excess electron energy with respect to E_F. The distributions were calculated for different energy values (in eV) of incident photons as indicated in the legend. (B) Fraction of the electron population with momenta within the escape cone ($P(k_x > k_s)$). Transmission coefficient $\langle T \rangle$ shown as a function of excess electron energy. (C) P_1: fraction of the electron population with energies above Φ_{SB} shown as a function of incident photon energy. P_2: is the fraction of the electron population with $E_e > \Phi_{SB}$ and with momenta within the escape cone. η_{inj} is the injection efficiency which corresponds to P_2 weighted by the transmission coefficient $\langle T \rangle$.

S3.1 $\eta_{\mathbf{inj}}$: Injection efficiency

The injection efficiency is the probability of photoexcitation of electrons (by way of surface plasmon relaxation) with kinetic energies in excess of the metal–semiconductor Schottky barrier and with sufficient momentum to traverse the barrier. Injection requires a non–vanishing transmission coefficient across the barrier.

S3.1.1 Energy distribution of photo–excited electrons

Illumination of the nanoparticles results in the excitation of surface plasmons. Non–radiative (Landau) dephasing of these excitations leads to the energy transfer from a surface plasmon (with energy $h\nu$) to a single electron hole–pair resulting in the excitation of electrons from below the Fermi level of the metal E_F with energies $E_F - h\nu < E_i < E_F$ to unoccupied states with energies $E_F + E_e$ with E_e being the excess kinetic energy of the electron where $0 < E_e < h\nu$. The energy distribution of these excited states has been argued to be almost uniform due to the fact that Landau damping occurs as intraband transitions between states of *sp* character that have constant energy–densities a few eV above and below the E_F for metals.[2]

Here, we take the approach described by White and Catchpole[3] to estimate the shape of the hot–electron energy density distribution $D(E_e; h\nu)$:

$$D(E_e; h\nu) \propto \rho(E_e - h\nu) f(E_e - h\nu) \rho(E_e) \left[1 - f(E_e)\right], \tag{S5}$$

where $\rho(x)$ is well approximated by the free–electron gas model, $\rho(x) \sim x^{1/2}$ and $f(x)$ is the Fermi–Dirac distribution function. This approximation does not take into account the conservation of momentum in the electronic transitions. The shape of this distribution is shown in figure S8(A) for four values of incident photon energy, assuming a metal work function of 5.1 eV and a Schottky barrier height of 1 eV. The shaded area in these curves correspond to the fraction of the resulting population with energies above the Schottky

barrier, a fraction shown *vs* $h\nu$ by curve P_1 in figure S8(C).

S3.1.2 Escape cone in momentum space

Let us consider the metal–semiconductor interface as consisting of an infinite plane in space. If we represent with x the axis normal to the interface, then a requirement for electron injection is that the x component of the electron momentum $k_{sx} = k_e \cos(\Omega_s)$ should have an associated energy larger than the Schottky barrier. This condition allows us to define an escape cone of angle Ω_s in k space by:

$$k_{sx} = k_e \cos(\Omega_s) = \sqrt{2m\Phi_{SB}}/\hbar. \tag{S6}$$

The fraction of the hot–electron population that posses x components of their momentum with an associated kinetic energy with sufficient magnitude to cross the interface, is given by the ratio of the solid angle subtended by Ω_s to the solid angle of the entire sphere of constant energy in k space (under the assumption of uniform distribution of momenta):

$$\begin{aligned} P(k_x > k_s) &= \frac{1}{4\pi} \int_0^{2\pi} \int_0^{\Omega_s} \sin(\theta) d\theta d\phi \\ &= \frac{1}{2} \left[1 - \cos(\Omega_s)\right] \\ &= \frac{1}{2} \left(1 - \sqrt{\frac{\Phi_{SB}}{E_e}}\right), \end{aligned} \tag{S7}$$

valid for $E_e > \Phi_{SB}$. This result shows that the fraction of hot–electrons moving to the flat metal–semiconductor interface asymptotes to 1/2 for the cases where $\Phi_{SB} \to 0$ or $E_e \gg \Phi_{SB}$. Figure S8(B) shows how this fraction of the hot–electron population varies with electron energy, whereas figure S8(C) shows the fraction of the population that meets both the energy and momentum requirements for electron injection (curve P_2).

When $D(E_e; h\nu)$ is an uniform distribution, it can be shown that the fraction of the hot–

electron population that has both the energy and momentum required for electron escape:

$$\int_{\Phi_{SB}}^{\infty} D(E;h\nu)P(k_x > k_s),$$

asymptotes to the Fowler equation.[4]

S3.1.3 Transmission coefficient

One more consideration to bear in mind is the possibility of reflections at the metal–semiconductor interface, which arises due to the possible mismatch between the momenta of the hot–electron in both media. On the metal side, the kinetic energy of the hot–electron is:

$$E_k = E_e = \frac{\hbar^2}{2m_e}\left[k^2\right], \tag{S8}$$

whereas on the semiconductor side it becomes

$$E_e - \Phi_{SB} = \frac{\hbar^2}{2m_e^*}(\kappa^2), \tag{S9}$$

where in general $m_e \neq m_e^*$. The transmission coefficient T at the interface is given by:[5]

$$\begin{aligned} T &= \frac{4k_{sx}\kappa_x}{m_e m_e^*(k_{sx}/m_e + \kappa_x/m_e^*)^2} \\ &= \frac{4k_{sx}\kappa\cos(\theta)}{m_e m_e^*(k_{sx}/m_e + \kappa\cos(\theta)/m_e^*)^2}, \end{aligned} \tag{S10}$$

where k_{sx} is given by Eqn. (S6) and we have considered only those hot–electrons within the escape cone subtended by Ω_s. T has been written in terms of the total momentum κ inside the semiconductor and the angle θ of its projection on the axis perpendicular to the interface (*i.e.* $\kappa_x = \kappa\cos(\theta)$).

In the work of Chalabi *et al*[6] it was assumed that due to the translation invariance of their metal–semiconductor interface along one direction, the momentum component parallel to the

interface k_y was conserved during the charge transfer process. This condition simplifies the calculation of the transmission probability of eqn. (S10), but it is a condition that may not be satisfied in general (e.g. for metal nanoparticles). A more general consideration consists on assuming conservation of the total momentum and accounting for possible changes in the direction of the momentum after injection: the electrons move away from the metal, or equivalently that the angle θ on eqn. (S10) varies from 0 to $\pi/2$. With this in mind, an angle–averaged transmission coefficient $\langle T \rangle$ can be calculated as follows:

$$\begin{aligned} \langle T \rangle &= \frac{1}{2\pi} \int_0^{2\pi} \int_0^{\pi/2} \frac{4\alpha \cos(\theta)}{(\alpha + \cos(\theta))^2} d\phi d\theta \\ &= 4\alpha \left[\ln\left(\frac{\alpha + 1}{\alpha} \right) + \frac{\alpha}{1+\alpha} - 1 \right], \end{aligned} \tag{S11}$$

where $\alpha = k_{sx} m_e^* / \kappa m_e = \sqrt{\frac{m_e^* \phi_b}{m_e (E_e - \Phi_{SB})}}$. This transmission coefficient is shown in figure S8(B) $\langle T \rangle$ assuming an Au–TiO_2 interface and a ratio for electron effective mass of 0.0862 (data taken from Zhang *et al*[7]). Similar results are reported by Nienhaus *et al.*[8]

The efficiency of hot–electron injection η_{inj} is then calculated as:

$$\eta_{\text{inj}}(h\nu) = \frac{\int_{\phi_b}^{\infty} dE D(E; h\nu) P(k_x > k_s) \langle T(E) \rangle}{\int_0^{\infty} dE D(E; h\nu)}. \tag{S12}$$

η_{inj} depends on the height of the Schottky barrier height Φ_{SB}, the incident photon energy $h\nu$, the ratio of electron effective masses in the metal and semiconductor material and the temperature. Figure S8(C) shows η_{inj}.

S3.2 η_{trpt}: Transport efficiency

This is the probability that an electron entering the semiconductor layer (of thickness t) traverses it without experiencing a scattering event (such as trapping at defect sites). This depends on the mean free path of charge carriers on the semiconductor material $l_{eff}(E_e)$,

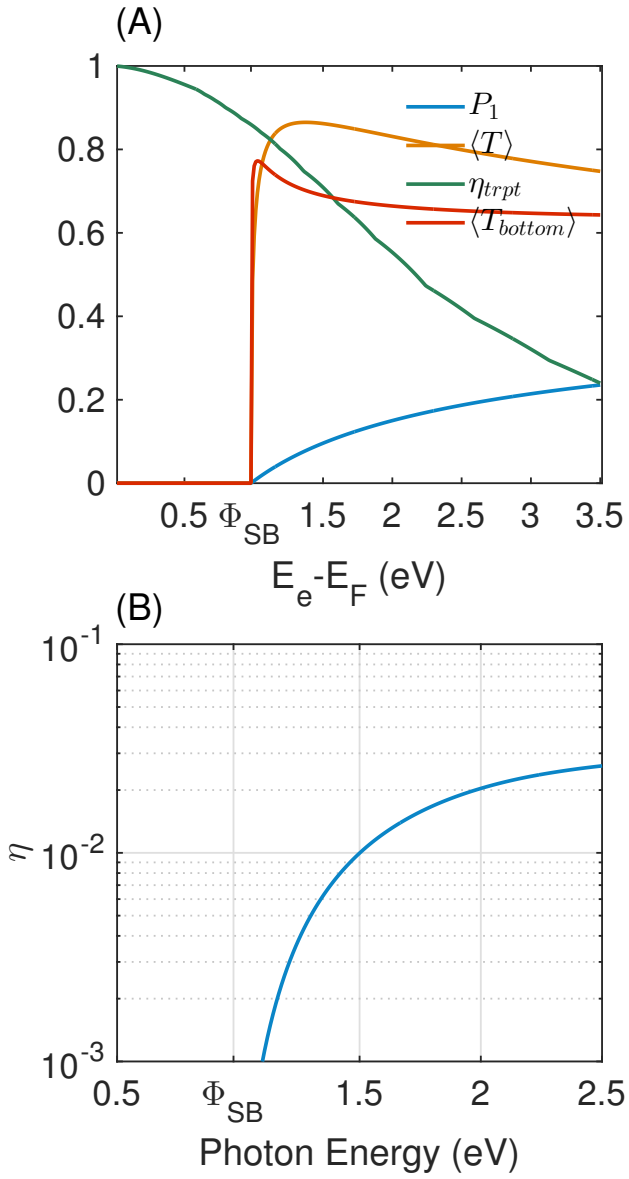

Figure S9: Internal quantum efficiency. (A) Plots of η_{trpt} and $\eta_{\text{injm}} = \langle T_{\text{bottom}} \rangle$ shown as a function of electron excess energy above the metal's Fermi level (E_F, in eV). For comparison, we also reproduce the curves P_1 and $\langle T \rangle$ of figure S9. (B) η vs incident photon energy for Φ_{SB}=0.98 eV

which, in turn, depends on the excess energy of the electron E_e:

$$\eta_{\text{trpt}}(E_e) = \frac{1}{t}\int_0^t \exp(-z/l_{eff}(E_e))dz. \tag{S13}$$

The mean free path for electrons in TiO_2 was obtained at each electron energy from the universal curve compiled in reference.[9] For a thickness of 50 nm, the transport efficiency is shown in figure S9(A), which clearly shows that high energy electrons experience more scattering.

S3.3 η_{injm}: Injection into metal reflector/mirror

This last step is dictated by the electron transmission probability at this final interface $\langle T_{\text{bottom}}\rangle$, which can be calculated in an analogous manner to what was described previously. Following this rationale, the angle–averaged transmission coefficient is given by:

$$\begin{aligned}\eta_{\text{injm}} &= \langle T_{\text{bottom}}\rangle \\ &= \frac{(2\beta^2+2)\ln(\beta+1) - 2\beta^2\ln(\beta) - 2\beta}{\beta},\end{aligned} \tag{S14}$$

where:

$$\beta^2 = \frac{m(E_e - \Phi_{SB})}{m^*(E_e - \Phi_{SB} - eV)}. \tag{S15}$$

where eV is the magnitude of the applied bias across the MSM junction. The magnitude of this transmission coefficient is shown in figure S9(A) ($\langle T_{bottom}\rangle$).

The internal quantum efficiency η is then calculated, as a function of incident photon energy as:

$$\eta(h\nu) = \frac{\int_{\phi_b}^{\infty} D(x;h\nu)P(k_x > k_s)\langle T(x)\rangle\eta_{\text{trpt}}(x)\langle T_{bottom}(x)\rangle dx}{\int_0^{\infty} dED(x;h\nu)}.$$

η is shown in figure S9(B). Figure S10 shows the expected effect of Φ_{SB} and semiconductor thickness on η. Similar lineshapes have been obtained by Leenheer *et. al*[10]

This model is expected to largely overestimate the IPCE at shorter wavelengths due to the fact that no attempt was made to consider possible photocurrent contributions due to the excitation of surface plasmon polaritons at the Au mirror/TiO_2 interface. As discussed in the main text and by Chalabi *et al*[6] and Wang and Melosh,[11] these currents will have an opposite sign to the ones produced by photoexcitation and plasmon decay by the metal nanoparticles.

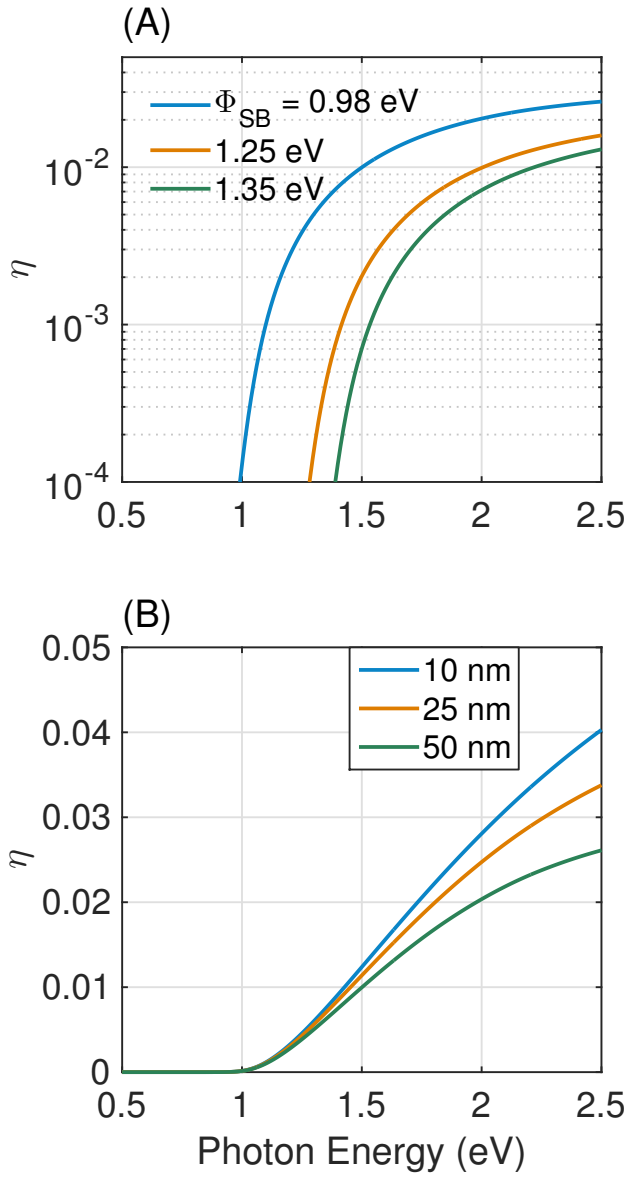

Figure S10: Effect of Schottky barrier height (A) and semiconductor thickness (B) on η

References

1. Palik, E., Ed. *Handbook of Optical Constants of Solids*; Academic Press, 1985.

2. Moskovits, M. Surface-Enhanced Spectroscopy. *Rev. Mod. Phys.* **1985**, *57*, 783–826.

3. White, T. P.; Catchpole, K. R. Plasmon-enhanced Internal Photoemission For Photovoltaics: Theoretical Efficiency Limits. *Appl. Phys. Lett.* **2012**, *101*, 073905.

4. Scales, C.; Berini, P. Thin-Film Schottky Barrier Photodetector Models. *IEEE J. Quant. Electron.* **2010**, *46*, 633–643.

5. Davies, J. H. *The Physics of Low-dimensional Semiconductors: An Introduction*; Cambridge University Press, 1998.

6. Chalabi, H.; Schoen, D.; Brongersma, M. L. Hot-Electron Photodetection with a Plasmonic Nanostripe Antenna. *Nano Lett.* **2014**, *14*, 1374 – 1380.

7. Zhang, J.; Zhou, P.; Liu, J.; Yu, J. New Understanding Of The Difference Of Photocatalytic Activity Among Anatase, Rutile And Brookite TiO_2. *Phys. Chem. Chem. Phys.* **2014**, *16*, 20382–20386.

8. Nienhaus, H.; Gergen, B.; Weinberg, W.; McFarland, E. Detection Of Chemically Induced Hot Charge Carriers With Ultrathin Metal Film Schottky Contacts. *Surf. Sci.* **2002**, *514*, 172 – 181.

9. Seah, M. P.; Dench, W. A. Quantitative Electron Spectroscopy Of Surfaces: A Standard Data Base For Electron Inelastic Mean Free Paths In Solids. *Surf. Interface Anal.* **1979**, *1*, 2–11.

10. Leenheer, A. J.; Narang, P.; Lewis, N. S.; Atwater, H. A. Solar Energy Conversion *via* Hot Electron Internal Photoemission In Metallic Nanostructures: Efficiency Estimates. *J. Appl. Phys.* **2014**, *115*, 134301.

11. Wang, F.; Melosh, N. A. Plasmonic Energy Collection through Hot Carrier Extraction. *Nano Lett.* **2011**, *11*, 5426–5430.